

Strong Gravitational Lensing and Dynamical Dark Energy

Andrea V. Macciò [★]

Institute for Theoretical Physics, University of Zürich, CH-8057 Zürich, Switzerland

Physics Department G. Occhialini, Università degli Studi di Milano-Bicocca, Piazza della Scienza 3, I-20126 Milan, Italy

INFN, via Celoria 16, I-20133 Milan, Italy

Draft version 2 December 2024

ABSTRACT

We study the strong gravitational lensing properties of galaxy clusters obtained from N-body simulations with different kind of Dark Energy (DE). We consider both dynamical DE, due to a scalar field self-interacting through Ratra–Peebles (RP) or SUGRA potentials, and DE with constant negative $w = p/\rho = -1$ (Λ CDM). We have 12 high resolution lensing systems for each cosmological model with a mass greater than $5.0 \times 10^{14} h^{-1} M_{\odot}$. Using a Ray Shooting technique we make a detailed analysis of the lensing properties of these clusters with particular attention to the number of arcs and their properties (magnification, length and width). We found that the number of giant arcs produced by galaxy clusters can change by an order of magnitude between Λ CDM models and Dynamical Dark Energy models with a RP potential. These differences originate from the different epochs of cluster formation and from the non-linearity of the strong lensing effect. We discuss the comparison with observational data.

Key words: methods: analytical — methods: numerical — galaxies: clusters: general — cosmology: theory — dark matter — galaxies: halos

1 INTRODUCTION

The mounting observational evidence for the existence of Dark Energy (DE), which probably accounts for $\sim 70\%$ of the critical density of the Universe (Perlmutter et al. (1999); Riess et al. (1998); Tegmark, Zaldarriaga, & Hamilton (2001); Netterfield et al. (2002); Pogosian, Bond, & Contaldi (2003); Efstathiou et al. (2002); Percival et al. (2002); Spergel et al. (2003)), rises a number of questions concerning galaxy formation. The nature of DE is suitably described by the parameter $w = p/\rho$, which characterizes its equation of state. The Λ CDM model ($w = -1$) was extensively studied during the last decade. Recently much more attention was given to physically motivated models with variable w (Mainini, Macciò, & Bonometto (2003a)), for which a number of N-body simulations have been performed (Klypin et al. 2003, KMMB03 hereafter, Dolag et al. 2003, Linder & Jenkins 2003, Macciò et al. 2003).

One of the main results of KMMB03 was that dynamical DE halos are denser than those with the standard Λ CDM one. In this work we want to analyze the impact of this higher concentration on the strong lensing properties of the cluster size halos.

As was first noted by Bartelmann et al. (1998) (for

OCDM, SCDM and Λ CDM cosmology) the predicted number of giant arcs varies by orders of magnitude among different cosmological models and, in fact, gravitational lensing is a powerful tool to inspect the cluster properties and thus constrain w . In order to produce highly distorted images from background sources, clusters must be compact enough, so that their central surface density is greater than the critical surface density for lensing. Moreover strong lensing is a highly non-linear effect so it is very sensitive to small differences in the concentration of the lens.

Here, using a Ray Shooting technique, we make a lensing analysis of dark matter halos extracted from N-body simulations of cosmological models with varying w arising from physically motivated potentials which admit tracker solutions. In particular, we focus on the two most popular variants of dynamical DE (Wetterich (1988); Ratra & Peebles (1988); Wetterich (1995)). The first model was proposed by Ratra & Peebles (1984, RP hereafter) and it yields a rather slow evolution of w . The second model (Brax & Martin (1999); Brax, Martin, & Riazuelo (2000); Brax & Martin (2000)) is based on potentials found in supergravity (SUGRA) and it results in a much faster evolving w . Hence, RP and SUGRA potentials cover a large spectrum of evolving w . These potentials are written as

$$V(\phi) = \frac{\Lambda^{4+\alpha}}{\phi^{\alpha}} \quad RP, \quad (1)$$

[★] andrea@physik.unizh.ch

$$V(\phi) = \frac{\Lambda^{4+\alpha}}{\phi^\alpha} \exp(4\pi G\phi^2) \quad \text{SUGRA.} \quad (2)$$

Here Λ is an energy scale, currently set in the range 10^2 – 10^{10} GeV, relevant for the physics of fundamental interactions. The potentials depend also on the exponent α . The parameters Λ and α define the DE density parameter Ω_{DE} . However, we prefer to use Λ and Ω_{DE} as independent parameters. Figure 10 in (Mainini et al. (2003b)) gives examples of w evolution for RP and SUGRA models. The RP model considered in this paper has $\Lambda = 10^3$ GeV. At redshift $z = 0$ it has $w = -0.5$. The value of w gradually changes with the redshift: at $z = 5$ it is close to -0.4 . The SUGRA model has $w = -0.85$ at $z = 0$, but w drastically changes with redshift: $w \approx -0.4$ at $z = 5$. Although the w interval spanned by the RP model covers values significantly above -0.8 (not favored by observations), this case is still important both as a limiting reference case and to emphasize that models with constant w and models with variable w produce different results even if average values of w are not so different.

2 N-BODY SIMULATIONS

The Adaptive Refinement Tree code (ART; Kravtsov, Klypin & Khokhlov 1997) was used to run the simulations. The ART code starts with a uniform grid, which covers the whole computational box. This grid defines the lowest (zeroth) level of resolution of the simulation. The standard Particles-Mesh algorithms are used to compute density and gravitational potential on the zeroth-level mesh. The ART code reaches high force resolution by refining all high density regions using an automated refinement algorithm. The refinements are recursive: the refined regions can also be refined, each subsequent refinement having half of the previous level's cell size. This creates a hierarchy of refinement meshes of different resolution, size, and geometry covering regions of interest. Because each individual cubic cell can be refined, the shape of the refinement mesh can be arbitrary and match effectively the geometry of the region of interest.

The criterion for refinement is the local density of particles: if the number of particles in a mesh cell (as estimated by the Cloud-In-Cell method) exceeds the level n_{thresh} , the cell is split (“refined”) into 8 cells of the next refinement level. The refinement threshold depends on the refinement level. For the zero's level it is $n_{\text{thresh}} = 2$. For the higher levels it is set to $n_{\text{thresh}} = 4$. The code uses the expansion parameter a as the time variable. During the integration, spatial refinement is accompanied by temporal refinement. Namely, each level of refinement, l , is integrated with its own time step $\Delta t_l = \Delta a_0 / 2^l$, where $\Delta a_0 = 3 \times 10^{-3}$ is the global time step of the zeroth refinement level. This variable time stepping is very important for accuracy of the results. As the force resolution increases, more steps are needed to integrate the trajectories accurately. Extensive tests of the code and comparisons with other numerical N -body codes can be found in Kravtsov (1999) and Knebe et al. (2000). The code was modified to handle DE of different types (Mainini et al 2003b & KMMB03).

We performed a low resolution simulation for each model with the following parameters: box size: $320 h^{-1}$ Mpc, number of particles: 128^3 , force resolution: $9.2 h^{-1}$ kpc. Inside each simulation we selected the four most massive clus-

Model	Λ (GeV)	Box (h^{-1} Mpc)	Np	Mass res. ($h^{-1} M_\odot$)	Force res. (h^{-1} kpc)
RP	10^3	320	521^3	2.03×10^{10}	4.8
SUGRA	10^3	320	512^3	2.03×10^{10}	4.8
Λ CDM	0	320	512^3	2.03×10^{10}	4.8

Table 1. Parameters of simulations

ters and re-run them with a mass resolution 64 times higher. At the end we have 12 lensing systems (each cluster can be seen by three different orthogonal directions) for each cosmological model, with a mass resolution of $2.03 \times 10^{10} h^{-1} M_\odot$ and a force resolution of $4.8 h^{-1}$ kpc. A complete list of simulation parameters is contained in table 1.

3 LENSING SIMULATIONS

In order to compute arc statistics for the models discussed above, we adopted a technique similar to the one originally proposed by Bartelmann & Weiss (1994). We center the cluster in a cube of $4 h^{-1}$ Mpc side length and study three lenses, obtained by projecting the particle positions along the coordinate axes. This grants us a total of 12 lens planes per model that we treat as though being due to independent clusters, for our present purposes.

We then divide the projected density field Σ by the critical surface mass density for lensing

$$\Sigma_{cr} = \frac{c^2}{4\pi G} \frac{D_s}{D_L D_{LS}}, \quad (3)$$

so obtaining the convergence k . Here c is the speed of light, G is the gravitational constant, while D_L , D_s , D_{LS} are the angular-diameter distances between lens and observer, source and observer, lens and source, respectively. In the following, we adopt $z_L = 0.4$ for the lens redshift; for a discussion about the value of z_s see the next section and the Figure 6 and 9. Once we set the lens and source redshift, the value of the angular diameter distance depends on the cosmological model. We detail this point in the next section.

In Figure 1 we show the convergence map for one of the cluster, whose length scale size is $4 h^{-1}$ Mpc. Let us underline that multiple images occur only if $\Sigma > \Sigma_{cr}$ (so $k > 1$), as in this case.

The deflection angle due to this 2D particle distribution, on a given point \vec{x} on the lens plane reads:

$$\vec{\alpha}(\vec{x}) = \sum_{j=1}^N \frac{4G}{c^2} \frac{m_j}{|\vec{x} - \vec{y}_j|}. \quad (4)$$

Here \vec{y}_j is the position of the j -th particles and N is the total number of particles.

As direct summation requires a long time, we sped up the code by using a P³M-like algorithm: the lens plane was divided into 128×128 cells and direct summation was applied to particles belonging to the same cell of \vec{x} and for its 8 neighbor cells. Particles in other cells were then seen as a single particle in the cell baricenter, given the total mass of the particles inside the cell.

The deflection angle diverges when the distance between a light ray and a particle is zero. To avoid this unwanted

feature we introduce a softening parameter ϵ in eq.(4); the value ϵ is tuned on the resolution of the current simulation.

We start to compute $\vec{\alpha}(\vec{x})$ on a regular grid of 128×128 test rays, then we propagate a bundle of 1024×1024 light rays and determine the deflection angle on each light ray by bicubic interpolation amongst the four nearest test rays.

The relation between images and sources position is given by the lens equation:

$$\vec{y} = \vec{x} - \vec{\alpha}(\vec{x}) \quad (5)$$

and the local properties of the lens mapping are then described by the Jacobian matrix of the lens equation,

$$A_{hk}(\vec{x}) = \frac{\partial y_h}{\partial x_k} = \delta_{hk} - \frac{\partial \alpha_h}{\partial x_k} \quad (6)$$

The shear components γ_1 and γ_2 are found from A_{hk} through the standard relations:

$$\gamma_1(\vec{x}) = -\frac{1}{2}[A_{11}(\vec{x}) - A_{22}(\vec{x})], \quad (7)$$

$$\gamma_2(\vec{x}) = -\frac{1}{2}[A_{12}(\vec{x}) + A_{21}(\vec{x})], \quad (8)$$

and the magnifications factor μ is given by the Jacobian determinant,

$$\mu(\vec{x}) = \frac{1}{\det A} = [A_{11}(\vec{x})A_{22}(\vec{x}) - A_{12}(\vec{x})A_{21}(\vec{x})]^{-1}. \quad (9)$$

Finally, the Jacobian determines the location of the critical curves \vec{x}_c on the lens plane, which are defined by $\det A(\vec{x}_c) = 0$. Because of the finite grid resolution, we can only approximately locate them by looking for pairs of adjacent cells with opposite signs of $\det A$. Then, the lens equations

$$\vec{y}_c = \vec{x}_c - \vec{\alpha}(\vec{x}_c), \quad (10)$$

yield the corresponding caustics \vec{y}_c , on the source plane.

3.1 Sources deformation

For statistical purposes one has to distribute and map a large number of sources. We are interested in arc properties and arcs form near caustics; so for numerical efficiency we have to distribute less sources in those part of the source plane that are far away from any caustics, and more sources close or inside the caustics. We follow the method introduced by Miralda-Escud  (1993) and later adapted to non-analytical models by Bartelmann & Weiss (1994). In the previous section we have obtained the deflection angles for the \vec{x}_{ij} (with $i,j=1,\dots,1024$) positions on the lens (or image) plane, using the lens equation (10) we can obtain the corresponding positions on the source plane $\vec{y}_{ij}(\vec{x}_{ij})$, as usual we call this discrete transformation the *mapping table*.

We model sources as circles with a radius $r_s = 1''$. We first distribute sources on a coarse grid of 32×32 , defined in the central quarter of the source plane covered by the light rays traced (due to convergence only a restricted part of the source plane can be reached by the light rays traced from the observer through the lens plane). From the mapping table we have obtained the magnification (μ), if it changes by more than one (absolute value) between two sources, we place an additional source between both, in this way we increase the resolution by a factor 2 in each dimension. For

Sat Feb 14 20:09:16 2004

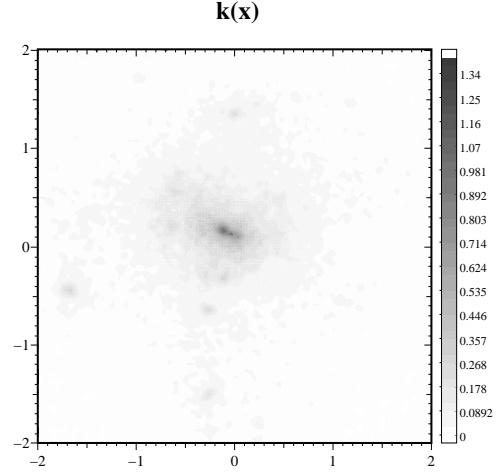


Figure 1. Convergence map for one of the Λ CDM clusters. The side length is $4 h^{-1}$ Mpc. In the central part $k > 1$, so this halo is able to produce giant arcs.

the n -th iteration of source positions the criterium to add additional sources is that magnification changes by 2^{n-1} . We repeat this procedure four times to obtain the final list of source positions. To compensate for this artificial increase in the source number density we assign a statistical weight of 2^{1-n} to each image of a source placed during the n -th grid refinement. On average we have about 5000 sources for each lensing system.

3.2 Arcs Analysis

To find the images of an extended source, all images-plane positions \vec{x}_{ij} are checked if the corresponding entry in the map table \vec{y}_{ij} lies within the source: i.e. for a circular source of radius r_s and center \vec{y}_c it is checked if:

$$(\vec{y}_{ij}(\vec{x}_{ij}) - \vec{y}_c)^2 \leq r_s^2. \quad (11)$$

Those points fulfilling the previous equation are part of one of the source images and are called image points. We then use a standard *friends-of-friends* algorithm to group together image points within connected regions, since they belong to the same image (the number of images of one source ranges from 1 to 5 for our cluster).

We measure arc properties using a method based on Bartelmann & Weiss (1994). The arc area and magnification are found by summing the areas of the pixel falling into the image. Arc lengths are estimated by first finding the arc center, then finding the arc pixel farthest from the centroid as well as the pixel farthest from this pixel. The arc length

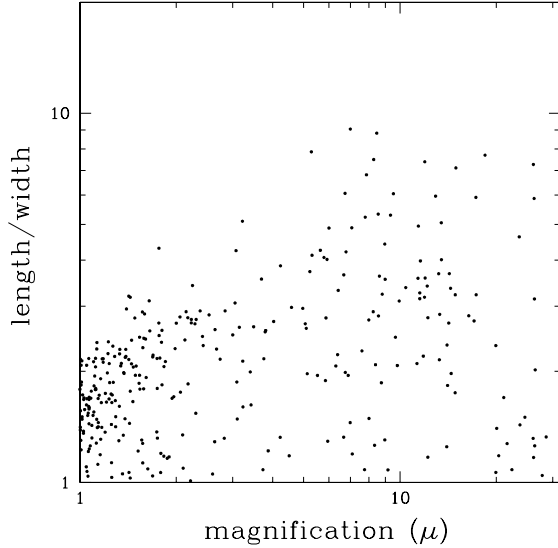


Figure 2. Magnification vs. length/width ratio for Λ CDM clusters. These two quantities are equal for an isothermal sphere lens.

is then given by the sum of the lengths of the two lines connecting these three points. The arc width is defined as the ratio between the arc area and the arc length.

In Figure 2 we plot the relation between length/width ratio and magnification; we found a good agreement with previous results obtained by Dalal et al. (2003). The scatter in this relation is due to local fluctuations in the surface mass density, highly distorted images are also highly magnified, but the converse is not always true.

4 ARCS STATISTICS

In this paper we aim to compare the lensing properties of a given cluster as it appears in different cosmological models. There are three main features that affect the number of giant arcs: the concentration of the halo, the total number of lensing systems at a given redshift and the value of the critical surface mass density (Σ_{cr}).

As first noted by KMMB03, and then confirmed by Dogut et al (2003) and Linder & Jenkins (2003), the concentration of dynamical DE halos is greater than the concentration of Λ CDM ones. Here we use the same definition of concentration of KMMB03: the ratio of the radius at the overdensity of the Λ CDM model (103 times the critical density) to the characteristic (“core”) radius of the NFW profile. (see however KMMB03 for more details). A greater concentration increases the probability of forming giant arcs. In Figure 3 we report the density profile of the same halo simulated in different cosmological models. The RP halo is clearly denser and more concentrated than the Λ CDM halo with the SUGRA halo laying in between.

The expected number of objects with a mass exceeding $4 \times 10^{14} h^{-1} M_{\odot}$ (in order to produce multiple images) at a given redshift (in this case $z = 0.4$) can be estimated using a Press & Schechter formalism (see Mainini et al 2003a). In dynamical DE, objects form earlier than in Λ CDM, so we

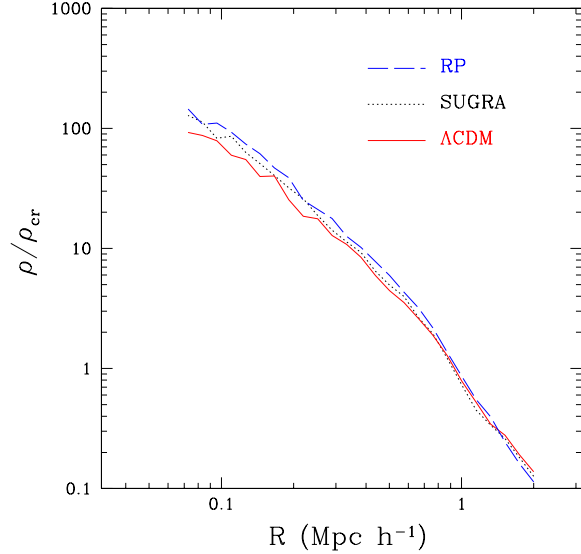


Figure 3. Density profile of the same halo simulated in different model. The red curve is for Λ CDM, the black one for SUGRA and the blue for RP. The halo has a virial mass of $6 \times 10^{14} h^{-1} M_{\odot}$.

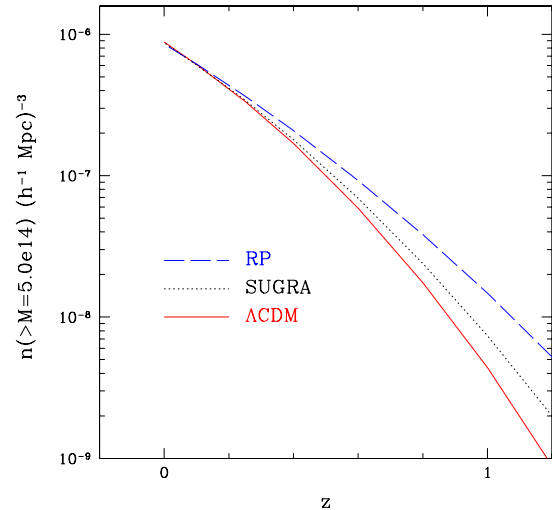


Figure 4. Number density of halos with a mass greater than $4.0 \times 10^{14} h^{-1} M_{\odot}$ for Λ CDM (lower curve), SUGRA (intermediate curve) and RP (upper curve). The value of Λ is 10^3 GeV for both RP and SUGRA.

have more lensing systems per Mpc^3 at $z = 0.4$. This can be taken into account by multiplying the number of arcs by 1.3 and 1.21, in RP and SUGRA respectively. (In Figure 4 we report the evolution with redshift of the mass function for a mass threshold of $4.0 \times 10^{14} h^{-1} M_{\odot}$.)

The evolution of the scale factor a with time also depends on the model. This implies that, at a given redshift $z = 1/a - 1$, the angular diameter distance D_{ad} is model dependent; in fact its value is given by:

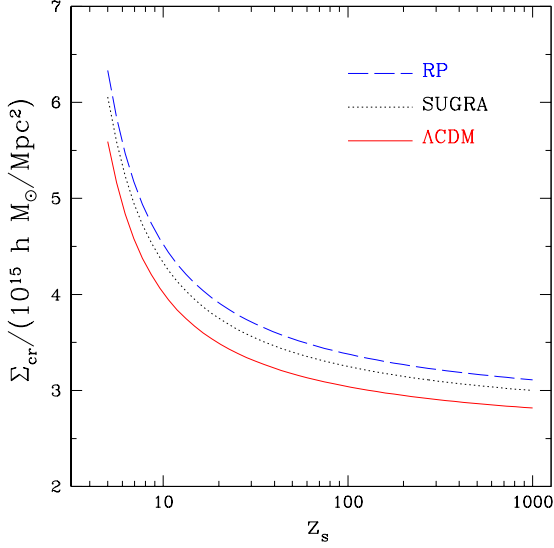


Figure 5. Value of the critical surface mass density Σ_{cr} in different cosmological models, for all the curves we choose a lens redshift $z_L = 0.4$

$$D_{ad}(a) = \frac{ac}{H_0} \int_a^1 \sqrt{\frac{a(1 - \Omega_{DE}(a))}{\Omega_{m,0}}} da. \quad (12)$$

Here c is the speed of light, H_0 and $\Omega_{m,0}$ are the present value of the Hubble constant and the matter density parameter and $\Omega_{DE}(a)$ gives the evolution of the DE density parameter with the expansion factor. To compute $\Omega_{DE}(a)$ for RP and SUGRA models we have used the analytical expression of Mainini et al (2003b). In Figure 5 we show the value of the critical surface mass density for the three adopted cosmological models. Recall that to obtain multiple images the surface density of the lens must exceed Σ_{cr} ; this means that a Λ CDM halo yields more arcs than a dynamical DE halo, if they have the same surface mass density. The effect of the different values of the angular diameter distance tends therefore to reduce the number of arcs in dynamical DE models.

The final result of our analysis are shown in Figure 6, where we plot the fraction of sources (number of sources divided by the total number) vs. their length/width ratio. As expected, the RP model produces more distorted images, due to its more concentrated halos. What is rather unexpected, instead, is that SUGRA and Λ CDM are similar. We argue that the effect of a bigger concentration is canceled by the increased Σ_{cr} value. As a further test we have computed the arc statistics in a SUGRA model using the Λ CDM critical surface density. As expected, we have obtained a result that is between RP and Λ CDM (Figure 7 dashed line).

As pointed out by many authors (Wambsganss et al. 2003, Dalal et al. 2003) the number of arcs that a cluster is able to produce is strongly related to the redshift of the sources (although the strength of this effect is not yet completely understood, different authors found different results). In Figure 8 we plot the arc number counts for the Λ CDM model for $z_s = 1$ (dashed line) and $z_s = 2$ (solid

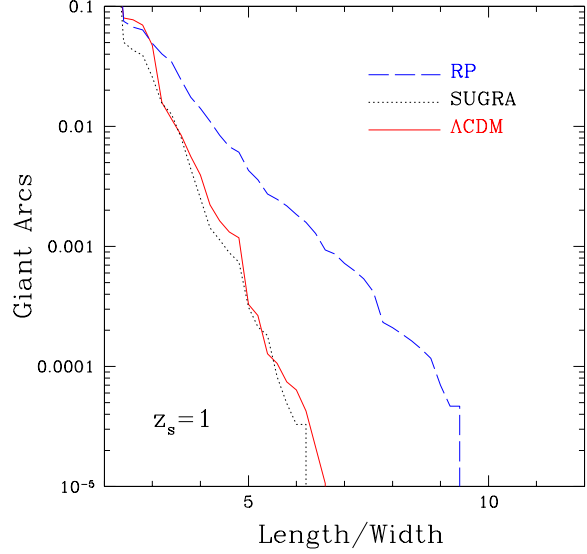


Figure 6. Fraction of sources mapped in an arc vs length/width ratio of the arc. Upper curve is RP (blue) than in red and black Λ CDM and SUGRA results respectively.

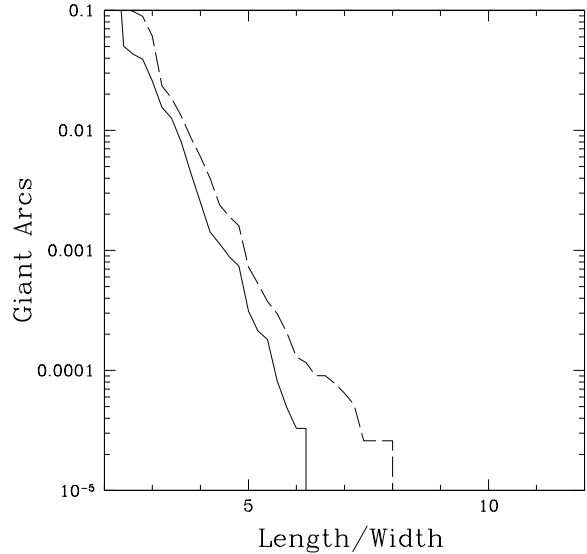


Figure 7. Same plot of Figure 6 for the SUGRA model where the arc properties are computed using $\Sigma_{cr}(\Lambda\text{CDM})$ (dashed line) and $\Sigma_{cr}(\text{SUGRA})$ (solid line).

line). As in previous work we found that the number of arcs increases if we increase the source redshifts.

Figure 9 shows the same results of Figure 6 but for $z_s = 2$. As expected, the total number of arcs increases in all cosmological models. Moreover, due to the low difference in the value of Σ_{cr} , the expected number of arcs is greater for SUGRA than for Λ CDM, with respect to the results obtained with $z_s = 1$.

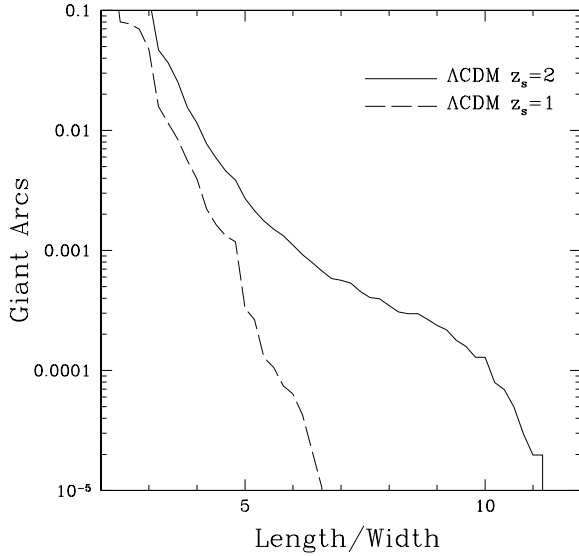


Figure 8. Arcs counts for different value of the source redshift in the Λ CDM model.

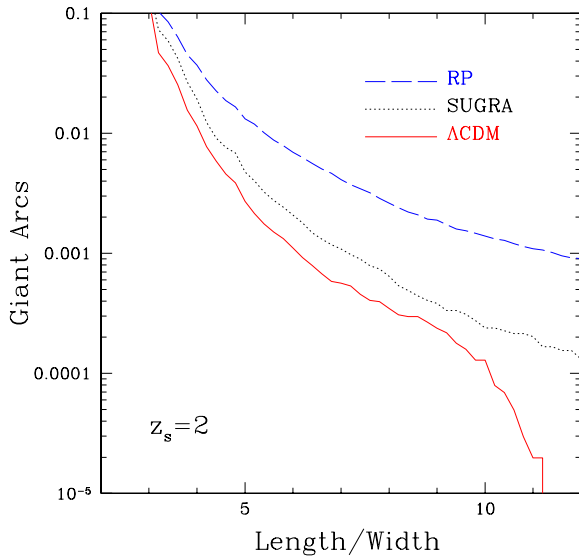


Figure 9. The same of Figure 6 for $z_s = 2$. With this value for the source redshift Λ CDM and SUGRA gives different results.

5 OBSERVATIONS

The comparison between observed instances of giant arcs and their predicted rate in the Λ CDM model has a long history. Bartelmann et al. (1998) found that the observational data exceeded the predicted number of giant arcs by an order of magnitude. This result was confirmed by other authors (Bartelmann et al. 2003; Meneghetti et al. 2003, 2001), but recent work suggests that the number of arcs found by Bartelmann significantly increases, if we allow for a broader range of source redshifts; in fact, the cross section to produce giant arcs is quite a steep function of the redshift (Wambsganss et al 2003).

Dalal et al (2003), using a larger sample of simulated Λ CDM clusters and an updated version of the EMSS lensing sample (Le Fevre et al. 1994, Luppino et al. 1999) have concluded that, at present, there is no discrepancy between the observed giant arc statistics and Λ CDM model predictions for $z \leq 0.6$. Another important issue that must be investigated, to make a detailed comparison of simulations with observations, is the role of cluster galaxies in the formation of giant arcs. Meneghetti et al. (2000), Flores et al (2000) and, especially, Meneghetti et al. (2003) found that cluster galaxies are generally unimportant, except for central cD galaxies, which can enhance the giant arc cross section by $\sim 50\%$.

A comparison between the results of the simulations considered here and available data is out of the scope of this paper. If Dalal et al (2003) is right, the arcs predicted by RP models exceed observations by more than one order of magnitude. On the contrary, the arcs predicted by SUGRA agree with observations. This model is also slightly favored in respect to Λ CDM for accounting of the small excess of giant arcs with wide separation, found at high redshift in the LCDSCS (Zaritsky & Gonzales 2003) and RCS (Gladders et al. 2003) samples.

6 DISCUSSION AND CONCLUSIONS

Models with dynamical DE are in an infant state. We do not know the nature of DE. Thus, the state parameter $w(t)$ is still uncertain. In view of this functional indetermination, at first sight, it could seem that the situation is hopeless.

In spite of that, we can outline some general trends that result from our analysis: in dynamical DE models, halos tend to collapse earlier than in a Λ CDM model with the same normalization at $z = 0$. As the result, halos are more concentrated and denser in their inner parts (KMMB03).

Starting from this finding we have explored the consequences of this higher concentration, on strong lensing properties of dark matter halos, in SUGRA and RP cosmologies. We found that RP halos produce a number of arcs an order of magnitude bigger than Λ CDM, regardless to the sources redshift. On the contrary, the SUGRA model is almost indistinguishable from Λ CDM, if the source redshift is set at $z_s = 1$, while it produces 2.5 times more arcs than Λ CDM, for a source redshift $z_s = 2$. This is due to the different evolution of the critical surface mass density with respect to z_s .

The Λ CDM scenario apparently agrees with current observations. If this is confirmed, a RP model with $\Lambda = 10^3$ GeV is ruled out by arc statistics. On the contrary, to discriminate between Λ CDM and SUGRA we need more extended observational surveys, like the CFHT Legacy Survey and the SDSS. They can be expected to improve the statistic of giant arcs on the sky. For example the RCS-2 Survey covers an area of 830 deg^2 and is expected to produce 50-100 new arcs. Such an observational material will provide a discrimination between Λ CDM and SUGRA and will possibly allow to constrain the Λ scale of the SUGRA potential.

ACKNOWLEDGMENTS

We thank Silvio Bonometto and Ben Moore for carefully reading the manuscript. We also thank INAF for allowing us to use the computer resources at the CINECA consortium (grant cnami44a on the SGI Origin 3800 machine).

REFERENCES

- Bartelmann M., Huss A., Carlberg J., Jenkins A. & Pearce F. 1998, *A&A* 330, 1
- Bartelmann M. & Weiss, A. 1994, *A&A* 287, 1
- Bartelmann M., Meneghetti, M., Perrotta F., Baccigalupi C. & Moscardini, L. 2003, *A&A* 409, 449B
- Brax, P. & Martin, J., 1999, *Phys.Lett.*, B468, 40
- Brax, P. & Martin, J., 2000, *Phys.Rev. D*, 61, 103502
- Brax P., Martin J. & Riazuelo A., 2000, *Phys.Rev. D*, 62, 103505
- Dalal, N., Holder, G. & Hennawi, J.F. 2003, *astro-ph/0310306*
- Dolag, K, Bartelmann M., Perrotta F., Baccigalupi C., Moscardini, L., Meneghetti, M. & Tormen, G. 2003, *astro-ph/0309771*
- Efstathiou, G. et al., 2002, *MNRAS*, 330, 29
- Flores, R.A., Maller, A.H. & Primack, J.R. 2000, *ApJ*, 535, 555
- Gladders, M.D., Hoekstra, H., Yee, H.K.C., Hall, P.B. & Barrientos, L.F. 2003, *ApJ*, 593, 48
- Klypin, A., Macciò A.V., Mainini R. & Bonometto S.A., 2003, *ApJ*, 599, 31
- Knebe, A., Kravtsov A., Gottlober, S. & Klypin A. 2000, *MNRAS*, 317, 630
- Kravtsov A., Klypin A. & Khokhlov A., 1997 *ApJ*, 111, 73 K
- Le Fevre et al. 1994, *ApJ*, 422, L5
- Linder E., & Jenkins A., 2003, *MNRAS*, 346, 573
- Luppino, G.A., Gioia, I.M., Hammer, F., Le Fevre, O. & Annis, J.A. 1999, *A&AS*, 136, 117
- Macciò A.V., Quercellini, C., Mainini R., Amendola, L. & Bonometto S.A., 2003, *astro-ph/0309671*, *Phys.Rev. D* (in press)
- Mainini R., Macciò A.V. & Bonometto S.A., 2003a, *NewA* 8, 172
- Mainini R., Macciò A.V., Bonometto S.A., & Klypin, A., 2003b, *ApJ*, 599, 24
- Meneghetti M., Bartelmann M. & Moscardini L. 2003, *MNRAS* 346, 67
- Meneghetti M., Yoshida, N., Bartelmann M., Moscardini L., Springel, V., Tormen G. & White, S.D.M. 2001, *MNRAS* 325, 435
- Meneghetti M., Bolzonella M., Bartelmann M., Moscardini L. & Tormen G. 2000, *MNRAS* 314, 338M
- Miralda-Escudè J. 1993, *ApJ*, 403, 497
- Netterfield, C. B. et al. 2002, *ApJ*, 571, 604
- Percival W.J. et al., 2002, *MNRAS*, 337, 1068
- Perlmutter S. et al., 1999, *ApJ*, 517, 565
- Pogosian, D., Bond, J.R., & Contaldi, C. 2003, *astro-ph/0301310*
- Ratra B., Peebles P.J.E., 1988, *Phys.Rev.D*, 37, 3406
- Riess, A.G. et al., 1998, *AJ*, 116, 1009
- Spergel et al. 2003, *astro-ph/0302209*
- Tegmark, M., Zaldarriaga, M., & Hamilton, A. J. 2001, *Phys. Rev. D*, 63, 43007
- Wambsganss, J., Bode, P. & Ostriker, J. P. 2003, *astro-ph/0306088*
- Wetterich C., 1988, *Nucl.Phys.B*, 302, 668
- Wetterich C., 1995 *A&A* 301, 32
- Zaritsky, D. & Gonzales, A.H. 2003 *ApJ*, 584, 691